



ELSEVIER

Journal of Materials Processing Technology 97 (2000) 158–167

Journal of  
**Materials  
Processing  
Technology**

www.elsevier.com/locate/jmatprotec

## Quality optimisation for laser machining under transient conditions

P. Di Pietro<sup>a,1</sup>, Y.L. Yao<sup>b,\*</sup>, A. Jeromin<sup>a</sup>

<sup>a</sup>*School of Mechanical and Manufacturing Engineering, The University of New South Wales, PO. Box 1, Kensington, NSW 2033, Australia*

<sup>b</sup>*Department of Mechanical Engineering, Columbia University 220 S.W. Mudd Building, New York, NY 10027, USA*

Received 21 July 1998

### Abstract

Quality improvements in laser machining have been achieved by a newly developed model-based optimisation strategy. The specific aims of such efforts are to assure machining quality right up to boundaries or pre-machined sections, which are inherent in intricate part geometry. Such boundaries frustrate heat-transfer and result in bulk heating of the workpiece. This in turn leads to a degradation of the machining quality. In order to achieve such optimisation, transient heat-transfer is modeled. Close inspection of the laser–workpiece interaction zone reveals that the machining front exhibits dynamic behaviour, and such mobility plays a significant role in temperature determination. Non-linear parameter adaption profiles are generated via the optimisation strategy in order to stabilise the machining front temperatures. Currently, trial-and-error based experimentation is needed in order to improve machining quality in such regions. Thus model-based optimisation has the added benefit of reducing this step whilst leading to an optimal solution. Experimental results are presented and it is demonstrated that such process manipulation can lead to significant quality improvements. © 2000 Elsevier Science S.A. All rights reserved.

*Keywords:* Laser machining; Model-based optimisation; Transient heat-transfer

### 1. Introduction

Today, laser machining of highly complex and intricate workpieces is a reality. Of concern though, is the effect of part geometry on the quality achievable. Such part geometry typically contains many pre-machined sections and boundaries, and heat accumulation is often severe. This can result in poor machining quality in the form of widespread burning, increased dross or debris, and increased surface roughness, amongst other problems.

In cases where heat fluxes are strong enough to melt the material, as in laser cutting, the problem becomes complex due to the moving solid–liquid interface. Efficient cutting occurs when the beam rides ahead on the unmolten material and therefore little energy falls through the generated cut.

When the cutting front speed increases due to heat accumulation, or when cutting at low processing speeds, the beam tends to lag behind the front. As a result, much more laser beam energy passes through the cut with little or no heating effect. Such characteristics of the process alter the amount of energy input into the interaction zone, and therefore the cutting front temperatures are expected to change. The generation of inconsistent cut quality can be attributed to such temperature deviations.

There have been many models developed over the years to describe the laser cutting process. A comprehensive review of these is given by the authors Di Pietro and Yao [1]. In particular, Gonsalves and Duley [2] first accounted for only part of the incident beam power being available for the laser cutting of sheet metals. This fraction was determined using a moving point source model. The model was used to determine the interrelationship between cutting speed, cut width and power required for efficient laser cutting. Powell et al. [3] devised cutting experiments to investigate the transmission and reflection losses occurring in the cutting process

\* Corresponding author. Tel.: +1-212-854-2887

E-mail address: ylyl@columbia.edu (Y.L. Yao)

<sup>1</sup> Currently Project Leader, Laser Processing, CSIRO Manufacturing Science and Technology, Australia.

based on previous work done by Miyamoto et al. [4,5]. It was shown that the amount of reflected/transmitted light reduced as sample thickness was increased. Schreiner-Mohr et al. [6] also conducted experimental work which showed that at maximum cutting speeds the beam centre can precede the front location. At low cutting speeds the beam centre was shown to lag behind the cutting front. A mono-dimensional finite difference model was proposed by Yuan et al. [7] which suggested that the cutting front could possess mobility when cutting at constant processing speeds. Arata et al. [8] showed through high speed photography that the cutting front was indeed dynamic in nature, and the formation of striations on the kerf walls could be explained well by the relative movement between the front and the laser beam.

Previous attempts at characterising the process have often assumed infinite workpiece length or they have prescribed fixed boundary temperatures. However, in the laser cutting of intricate parts, this assumption leads to low heat accumulation estimates. A transient model is therefore developed to account for workpiece geometry and the presence of a kerf is considered, with nodal points within it becoming part of the convective environment. Inherent problems associated with a moving cutting front and temporal variations of the energy input per unit time are resolved, including not only transience in the absorbed beam power because of coupling issues but also in the exothermic reaction energy.

## 2. Model-based optimisation

A complete description of the modeling has been presented elsewhere by the authors, Di Pietro and Yao [9] and a summary thereof is included in Appendix A for self-containment purposes. A brief summary of model-based optimisation is given below.

Industry [10] and other research groups realised early on that adaptive control of laser parameters was a real possibility with conventional computer numeric control (CNC) systems. By adapting parameters such as laser power levels, switching between continuous wave (CW) and pulsed mode, and effecting cutting speed changes, significant quality improvements were obtainable. Such techniques are trial-and-error based, and therefore are time consuming, whereby the optimal set of parameters may still not be reached. It was recognised by Biermann and Geiger [11] that simulation of the laser process under the effects of the motion system can lead to improved results for laser processing.

An optimisation strategy is therefore proposed in which it forces the cutting front temperature to remain steady right up to a prescribed boundary. The problem of minimising the deviation from steady-state results in a non-linear power profile, as the inter-relationships between laser parameters are complicated by the mobility exhibited by the cutting front. Uniform cutting front temperatures affect the quality in various ways. They produce better quality by maintaining kerf widths more consistently, producing more uniform

heat-affected zones, and reducing the amount of wide-spread self-burning. In a word, uniform cutting front temperatures reduce the variability in cut quality.

The strategy developed is iterative by nature. The model proceeds forward in time by the accumulation of the time-step  $t$  of integration. By monitoring the status of the front temperature at every instance, a steady-state value can be established. The cutting front temperature can only be disturbed subsequently by a boundary encroachment or by a speed change of the motion system. As the change in temperature remains less than the previously set limit  $T$ , that is,  $|T_f^{j+1} - T_f^j| < \Delta T$  where  $T_f$  denotes cutting front temperature and  $j$  current time, no action is taken. As the change in temperature exceeds  $T$ , a course of action is required in the form of a power rise or reduction of size  $P = |T_f^{j+1} - T_f^j|k$ . A conditional test is given: if  $T_f^{j+1} > T_f^j$ , then  $P_{inc}^j = P_{inc}^j - P$  where  $P_{inc}^j$  is incident beam power. Otherwise,  $P_{inc}^j = P_{inc}^j + P$ . From which, an updated cutting front temperature  $T_f^{j+1}$  is determined. If it falls within the set allowable temperature tolerance  $T_f^{j+1} \pm T$ , then the model proceeds forward to the next user-specified beam position, whereby the procedure repeats. If it still falls outside of the tolerance, the constant  $k$  is typically doubled (it is chosen arbitrarily as the beginning). If it is found that the new  $T_f^{j+1}$  overshoots, it will be reduced to three-fourths of itself. The process repeats until the tolerance is satisfied. The assumption that the required power change is proportional to the temperature difference is reasonable because the step size chosen is small.

## 3. Numerical issues

The determination of the mass removal rate is dependent upon firstly evaluating the cutting front speed. From Fig. 1, it can be shown that:

$$S_f = S_b - S + (S + S) = S_b + S, \quad (1)$$

where  $S_f$  is the distance that the front has moved from its previous location.  $S_b$  the distance the beam has moved from its previous location,  $S$  the molten layer thickness, and  $S$  the change in the molten layer thickness from that of the previous location. In the time interval  $t$ , an expression for the front velocity can be ascertained:

$$S_f/t = S_b/t + S/t. \quad (2)$$

The limit as  $t \rightarrow 0$ , yields the following instantaneous rates of change:

$$S_f/t = S_b/t + S/t, \quad (3)$$

from which Eq. (2) can be expressed in the general form:

$$V_f = V_b + S/t, \quad (4)$$

where  $V_f$  is the velocity of the cutting front,  $V_b$  the velocity of the laser beam, and  $S/t$  the time rate of the change of the molten layer thickness.

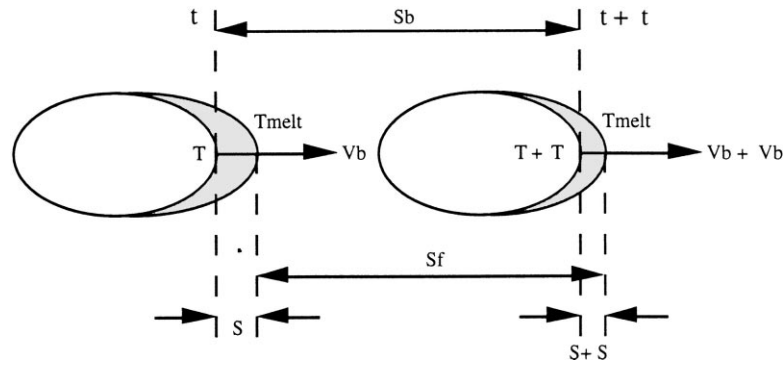


Fig. 1. Schematic diagram of the mobility of the cutting front over a time interval.

The molten layer thickness is given by the shortest distance from the melting isotherm to the laser beam's centre at any given time  $t$ . The melting isotherm then represents the solid–liquid interface. A numerical expression for the average time rate of change of the molten layer thickness over the interval  $t$  can be obtained for evaluating the front velocity. This is done by using a method of first-order interpolation between the nodal temperature  $T_m$  and the forward-shifted temperature  $T_{m+1}$ . At time  $t = j$ :

$$S^j = (y(T_m^j - T_{\text{melt}})) / (T_m^j - T_{m+1}^j), \tag{5}$$

where  $m$  denotes the nodal point of interest in the  $y$  direction. By analogy, at time  $t + t = j + 1$ :

$$S^{j+1} = (y(T_m^{j+1} - T_{\text{melt}})) / (T_m^{j+1} - T_{m+1}^{j+1}), \tag{6}$$

from which:

$$S/t = (S^{j+1} - S^j) / t. \tag{7}$$

The percentage of power incident on the workpiece is therefore given by the proportion by which the cutting front is ahead of the trailing edge of the laser beam, refer to Fig. 2. If the front is behind the trailing edge of the laser beam, then all of the beam power will fall on to the workpiece. This represents the most efficient beam coupling theoretically possible. In reality though, some beam leakage will always occur. After material is expelled from the kerf, conduction cannot occur across this region as these points are now part of the convective environment. The model accounts for this by removing all nodes above the

melting point which fall within the extent of the assist gas stream.

Heat diffusion equations are determined for all nodal points within the control volume and at boundaries. These balance equations can be solved in a number of ways. Implicit formulations were chosen because they have unlimited numerical stability. All nodes were swept by their appropriate equations until the temperatures converged to some previously set limit (refer to Appendix B).

On most occasions, it is necessary to initiate a keyhole in the work material prior to cutting. This issue is considered so that a realistic cutting process is simulated. Molten material can only be ejected upwards in all directions until complete penetration. The model can be used to obtain the minimum penetration times required to create such initiation holes, but to obtain more accurate penetration times, it is necessary to consider the formation of surface plasma [12]. Once a kerf is formed, the effect of these plasmas are reduced somewhat due to the ability of the gas jet to remove them more effectively. Surface plasmas are neglected in this model as the main emphasis is to simulate the cutting process as opposed to the drilling process.

Once all the discretised equations have converged, the model determines the current front velocity, from which the exothermic power can be calculated. The percentage of transmitted power lost through the kerf is then evaluated. The status of the current laser beam position relative to the workpiece is updated and a new time-step of integration is obtained. The model then loops and the procedure is repeated until the laser beam reaches its user-specified final

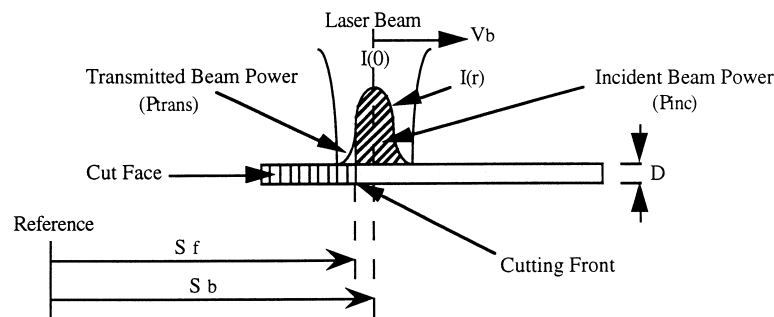


Fig. 2. Laser beam absorption and transmission losses in laser cutting.

stopping position, or until the front temperatures fall below melting point: this latter indicates that cutting conditions are poor and that quality can no longer be assured.

#### 4. Experimental procedure

The experiments were performed on a fast axial flow 1.5 kW CO<sub>2</sub> laser (PRC model FH 1501). The beam mode is essentially TEM<sub>00</sub>, with all experiments performed under CW operation. The laser beam was focussed down to 250 μm, through a 5" ZnSe high pressure meniscus lens. The throat diameter of the nozzle used was 1 mm, and a nozzle-standoff distance of 1 mm was maintained. The assist gas pressures were kept constant at 2.7 bar throughout the experiments. The cutting speed varies from 10 to 100 mm/s with increments of 10 or 20 mm/s. The laser power varies from 500, 600 to 800 W.

Cold-rolled mild steel plates (AS 1595) of 1 mm thickness were guillotined into 20 mm square blanks. Cuts were initiated 5 mm in from one end, and cut down the centreline of the workpiece of the other end (Fig. 4). All initiation keyholes were created by blast drilling with oxygen for a penetration period of 100 ms.

In order to validate calculated workpiece temperature distributions by those determined experimentally, type K, chromel–alumel thermocouples were used. An overall diameter of 0.5 mm with a response time of 50 ms was chosen, because thicker diameter thermocouples result in slower response time (typically 100 ms). The thermocouples were imbedded at various positions on the workpiece. These positions were chosen to avoid high temperature gradients closer to the line of cut and as such, allow the thermocouples to respond adequately (Fig. 4). At temperature of around 1273 K the thermocouple arms will oxidise, causing a change in their constituency and hence a change in EMF, so the temperatures need to remain below this threshold. In addition, validation becomes difficult at very close positions to the line of cut because small shifts in thermocouple locations results in large variations. This is due to the large temperature gradients experienced around the interaction zone. The thermocouple positions were accurately checked using a microscope and data collection was triggered via an electrical relay in the controller which actuates the beam shutter mechanism.

Polymethylmethacrylate (PMMA) was used to validate the transmitted power levels determined from the model. Acrylic blocks (approx. 25 mm square by 60 mm long) were placed 3 mm below the mild steel samples to obtain the burn prints. A strong air jet was used to remove the vapours produced while printing on the acrylic blocks was obtained. A specific ablation energy of 3000 J/cm<sup>3</sup> for PMMA was established by Miyamoto et al. [4]. Therefore by knowing the volume removed from the acrylic, together with the total time taken for the cut, the power losses through the kerf can be ascertained.

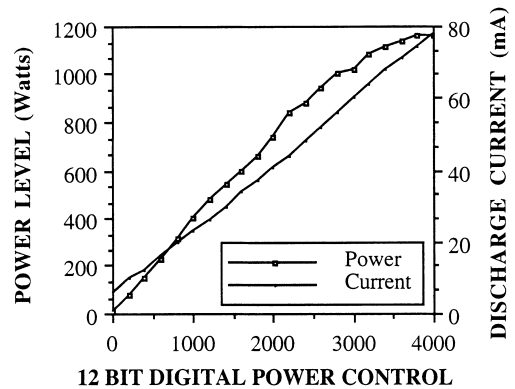


Fig. 3. Actual power levels obtainable as a function of discharge current and digital control word (power probe exposure time: 20 s, gas consumption rate: 150 l/h).

High speed photography was also undertaken to examine and investigate cutting front mobility on approach to a workpiece boundary. Cine films were taken at a camera speed of 500 frames per second, and the camera (HITACHI '16HM-HIMAC') was focussed directly on the laser–material interaction zone. It was positioned perpendicular to the line of cut at an angle of 15°, so that any lateral movement of the front in the direction of cut could easily be discerned. Analysis of the developed film was carried out under a Nikon shadowgraph, so that a large magnification of the front was possible. A Mitutoyo digital micrometer heads facilitated accurate measurements of any movements observed.

Actual power levels is calibrated for accurate model validation. Fig. 3 shows the power levels measured by a power probe and its associated discharge current for one of eight discharges. The current control is via a 12 bit digital word, which allows accurate manipulation through the part programs generated.

## 5. Results and discussion

### 5.1. Steady-state behaviour

To validate the simulated temperature distributions, the thermocouples were imbedded 2 mm in from the corner of the workpiece closest to the initiation point in both the *x* and *y* directions (Fig. 4). For precise analysis of the results, the thermocouples were calibrated directly against an accurate industrial oven.

Fig. 5 shows typical results obtained from model execution as compared to experimentally determined values from the thermocouples. Different cutting speeds and power levels were validated, and the close correlations suggest that the thermocouples were able to respond fast enough to validate the simulation results.

Fig. 6 shows the evaluation of total power losses obtained from the PMMA experiments as compared with the simula-

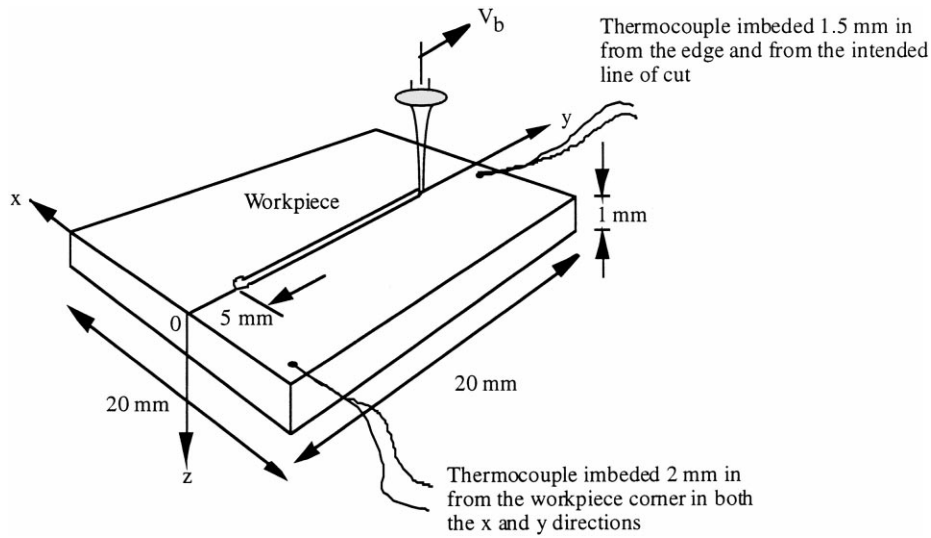


Fig. 4. Workpiece control volume and conditions.

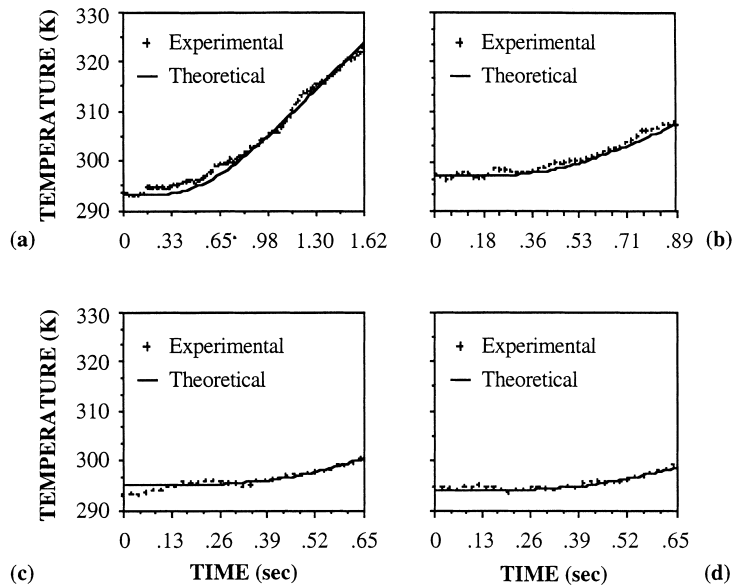


Fig. 5. Typical thermocouple temperature measurements obtained 2 mm in from the workpiece corner nearest the initiation point in both the x and y directions: (a) 600 W, 10 mm/s; (b) 600 W, 20 mm/s; (c) 600 W, 30 mm/s; (d) 500 W, 30 mm/s.

tion result at a constant laser power of 600 W. It is seen that with speed increases, the amount of power lost through the kerf decreases. This indicates that the cutting process is more efficient at higher processing speeds due to better beam coupling with workpiece material. The beaming coupling in percentage shown in Fig. 7.

5.2. Transient effects on boundary encroachment

Fig. 8 shows the results obtained from a simulation when no control strategy was implemented and run at a power setting of 600 W and a processing speed of 20 mm/s. Although the cutting speed  $V_b$  remains constant right up to the workpiece edge, the front velocity  $V_f$  begins to move

on its approach to the boundary because heat diffusion is frustrated and over-heating of the area occurs. The increase in the front speed produces an increase in the exothermic power, but this increase in contrast, also results in more power falling through the kerf. The net effect of all these mechanisms working at once is best depicted by the increase in the cutting front temperature experienced by the boundary encroachment.

5.2.1. Visualisation of cutting front mobility through high speed photography

High speed photography was undertaken in order to examine transient effects on approach to a boundary. The camera is fixtured with the laser coordinate system and

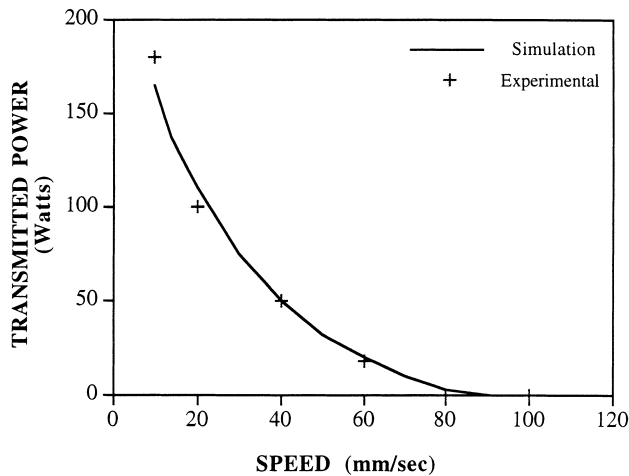


Fig. 6. Comparing steady-state power losses determined from the PMMA burn prints with simulated transmitted power levels. (laser power: 600 W).

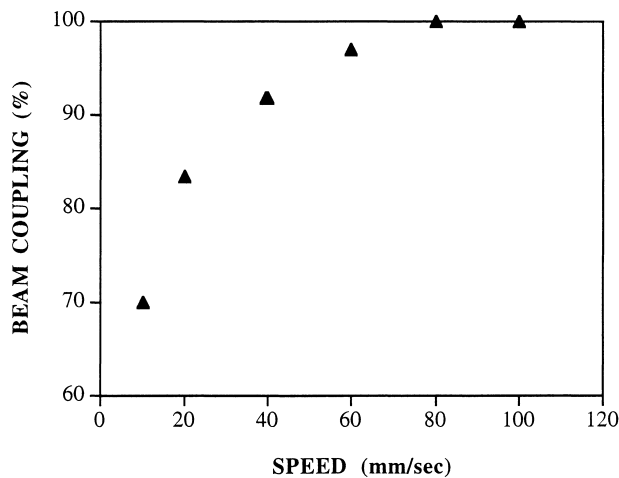


Fig. 7. Percentage beam coup (laser power: 600 W).

therefore sees no process change if the process remains steady-state. Fig. 9 shows a portion of the film when a cut boundary is encroached by the laser (under the same parameters used in the simulation, i.e., 600 W and 20 mm/s). The frame interval is 2 ms and therefore the portion covers about 0.3 mm from the boundary. The last photograph actually on the boundary (at +14 ms) is omitted because it was of poor quality, as self-burning of the workpiece occurred and resulted in a strong light emission, which obscured the cutting front.

Although the resolution of the film is limited, the relative changes between consecutive frames can be reasonably measured by a shadowgraph using a higher magnification. It is clear that as the cut proceeds closer to the prescribed boundary, the molten front speed  $V_f$  increases relative to the constant beam velocity  $V_b$ , as predicted in the simulation. By measuring the relative distance moved by the front between frames and knowing the camera speed, an approximate measure of the molten front speed could be determined,

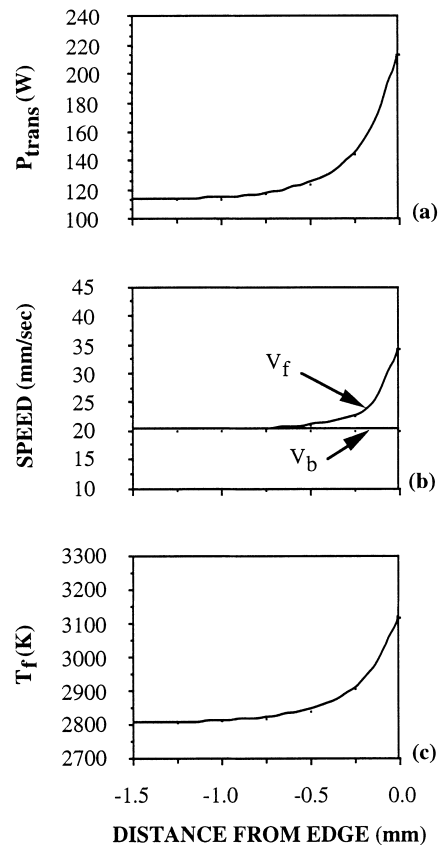


Fig. 8. The effect of boundary encroachment on: (a) transmitted power; (b) cutting front mobility; and (c) cutting front temperature (cutting speed: 20 mm/s, laser power: 600 W).

refer to Fig. 10. As seen, the values of increase in the molten front speed on approach to the workpiece edge are comparable to those determined in the simulation. Please note the values were only evaluated over the final 0.3 mm because the periodic front motion ceased from this point onwards and so provided a clear picture of the dynamics in this region. Prior to this stage, the cyclic nature of the light emission tended to dominate the cutting mechanism and no gradual increase in the front speed was evident. The cyclic nature is thought to be related with striation phenomenon [13].

### 5.2.2. Temperature growth on boundary encroachment

The temperatures occurring in the vicinity of the interaction zone (especially when the laser beam reaches a boundary) are important because they affect the quality of cut considerably. Although direct measurement of the molten front temperature is preferred, the harsh environment found under the nozzle (viz. space restrictions and high temperatures) makes this difficult. Non-contact pyrometric measurements have been attempted by the authors, but absolute temperature values are not possible and the dependence on constant emissivity and low response time amongst other factors led to the abandoning of this approach. Instead, thermocouple measurements were reverted to. These were imbedded 1.5 mm in from the prescribed boundary and

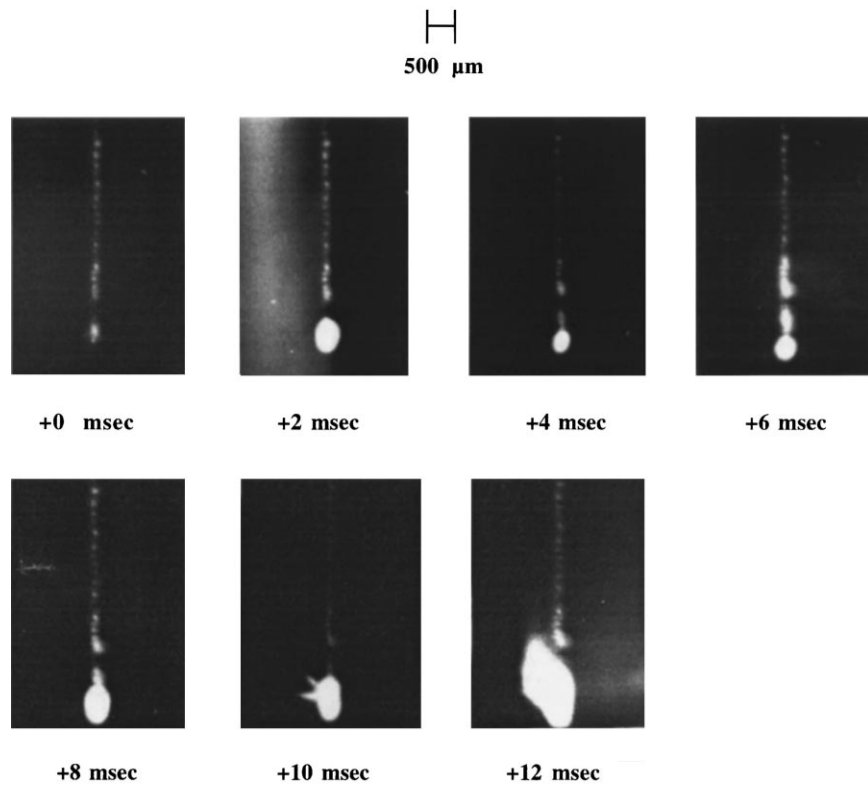


Fig. 9. Photographs taken under boundary encroachment conditions showing the forward motion of the molten front relative to the laser coordinate system to which the high speed camera is attached (cutting speed: 20 mm/s, laser power: 600 W).

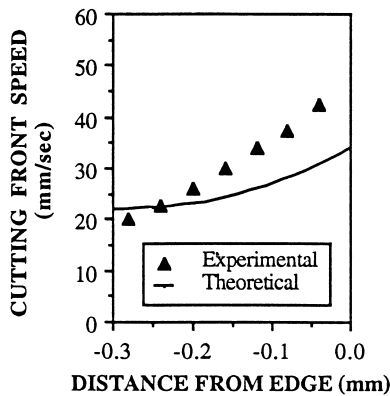


Fig. 10. Comparing theoretical and experimental cutting front mobility on approach to a workpiece boundary based on visualisation of the interaction zone (cutting speed: 20 mm/s, laser power: 600 W).

1.5 mm in from the intended line of cut (Fig. 4). Again, closer positions to the interaction zone led to poor thermocouple response and small deviations in location produced erroneous results because of the large temperature gradients experienced about the interaction zone.

Fig. 11 shows typical transience experienced in practice on approach to a prescribed boundary as compared to numerical results. Again the cutting parameters used were 600 W and 20 mm/s. Time histories of this temperature location are shown, and they can be seen to correlate well.

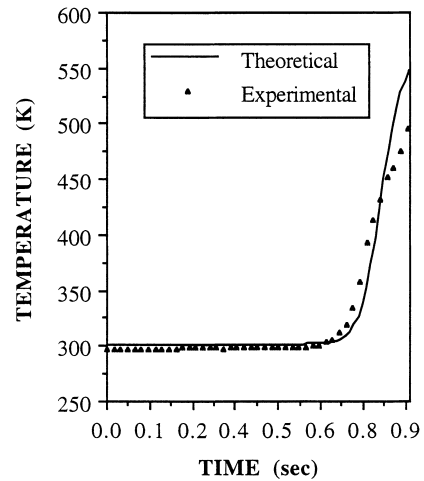


Fig. 11. Typical thermocouple temperature measurement imbedded 1.5 mm in from the boundary edge and from the line of cut as compared to the numerical solution (cutting speed: 20 mm/s, laser power: 600 W).

As the beam approaches the boundary, conduction is frustrated and results in wide-spread bulk heat and accumulation, causing the temperatures in this region to soar. This is evident from both the experimental and numerical results. Such large transient effects at this position only highlights that the actual cutting front must experience even more severe transience under the same conditions.

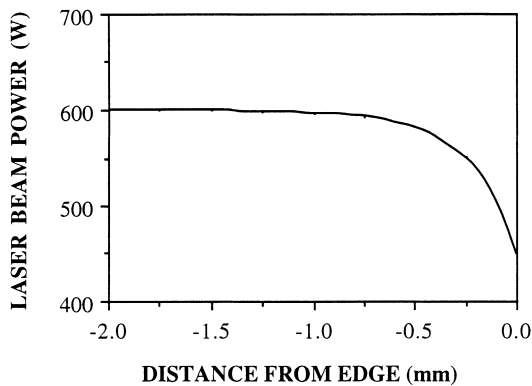


Fig. 12. Laser beam power profile required for temperature stabilisation on boundary encroachment (cutting speed: 20 mm/s, initial laser power: 600 W).

### 5.2.3. Power manipulation for quality improvements

Fig. 12 shows the power profile determined by the model-based optimisation strategy for temperature stabilisation when cutting with 600 W at 20 mm/s. To implement this optimisation strategy, tests were performed to determine the response time of the laser system to step inputs. The laser in use has current control and power control but needs to respond fast enough to closely approximate the theoretical profile.

Fig. 13 shows the response of a resonator discharge to a step input. A power change from 0 to 1000 W was commanded via the controller. The signal was obtained from a receptacle located on the discharge current meter. The output approximates a step response of a first-order system with a time constant of 1.3 ms. After two time constants, the response had all but reached its final value. Thus the laser control facility was adequate to perform the optimisation power strategies discussed.

Fig. 14 shows photographs taken of the kerf produced with and without power control for the conditions of 800 W and 30 mm/s. It is clear from the photographs that the quality of the cut at the beam exit is greatly improved by the control scheme. Ideally, no kerf widening should be observable under the power profiles adopted, but assumptions and simplifications in the model and the ability of the

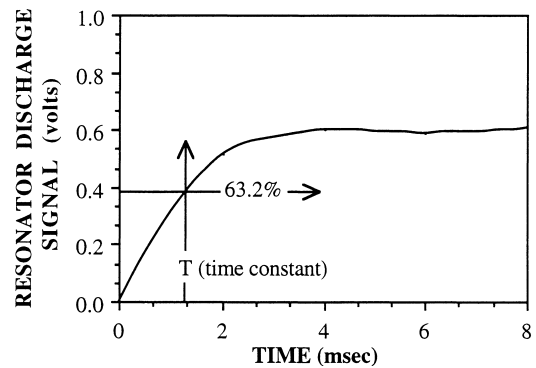


Fig. 13. Response curve of the discharge current subjected to a large step input from zero beam power to 1 kW.

laser to respond to such commands result in some quality deviations.

## 6. Conclusions

A model-based optimisation strategy for improving laser cutting quality of thin plate is presented. It is based on a numerical description of the process, which accounts for the fact that the front can exhibit mobility on approach to a prescribed boundary. It endeavours to manipulate laser beam power in order to stabilise the cutting front temperature right up to such pre-cut sections. This eliminates the need for the trial-and-error based experimentation that is adopted currently. First results obtained from the control scheme show significant improvement in quality through reduced kerf widening effects. PMMA burn prints also gave an insight into the power losses experienced in the laser cutting process. It was shown that although transmission and reflection mechanisms are identifiable during the reactive gas cutting of steel, reflection losses are minimised at high processing speeds. Actual visualisation of the dynamic front was achieved through high speed photography, and the results clearly show that mobility occurs under the effect of a boundary encroachment.

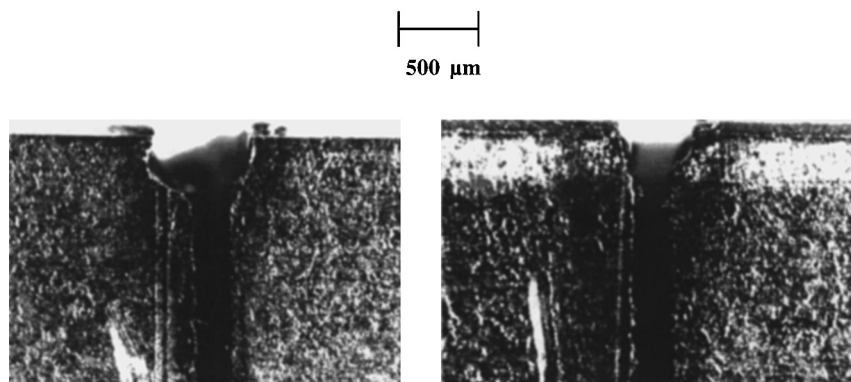


Fig. 14. Comparing the obtainable quality at the boundary: (a) without power adaption; (b) with power adaption (30 mm/s, 800 W).

## Acknowledgements

The authors gratefully acknowledge the support given by the Australian Research Council. Valuable discussions and assistance with the experiments given by Mr R. Fowle, Mr A. Harris and Dr A. Black from the School of Mechanical and Manufacturing Engineering, The University of New South Wales, Australia, are also duly acknowledged.

## Appendix A.

A brief summary of the mathematical formulation is given below. In order to focus on the development of optimisation, constant thermo-physical properties and two-dimensional transient heat conduction are simply assumed, whilst boundary conditions that allow convection and radiation to occur to the surroundings are considered. This results in the following equation:

$$\frac{K}{\rho c_v} \left( \frac{\partial^2 T}{\partial x^2} + \frac{\partial^2 T}{\partial y^2} \right) + \frac{\partial T}{\rho c_v \partial z} (h_f + h_n + 2h_r) + \frac{\dot{q}}{\rho c_v} = \frac{\partial T}{\partial t}, \quad (\text{A.1})$$

where  $K$  is the thermal conductivity,  $\rho$  the density,  $C_v$  the heat capacity,  $h_n$  the natural or free convective heat-transfer coefficient,  $h_r$  the radiative heat-transfer coefficient, and  $\dot{q}$  is the heat generation. The forced convective heat-transfer coefficient is:

$$h_f = \text{Nu}_d K / d, \quad (\text{A.2})$$

where  $d$  is the diameter and the Nusselt number determined using the Dittus–boelter formula [17] as:

$$\text{Nu}_d = 0.027 \text{Re}_d^{0.8} \text{Pr}^{0.33} (\mu_m / \mu_w)^{0.14}, \quad (\text{A.3})$$

where  $\text{Re}$  is the Reynolds number, and  $\text{Pr}$  the Prandtl number, and  $\mu_m$  and  $\mu_w$  are the mixed-mean and wall coefficients of viscosity. Although the free convection contribution  $h_n$  is relatively small, it is included also for the sake of completeness.

In Eq. (A.1), the radiative heat transfer coefficient  $h_r$  is given as:

$$h_r = \epsilon \sigma_b (T_b + T)(T_b^2 + T_\infty^2), \quad (\text{A.4})$$

where  $\epsilon$  is the emissivity,  $\sigma_b$  the Stefan–Boltzmann constant,  $T_b$  the boundary temperature, and  $T_\infty$  the ambient temperature. Because of the higher-order relationship in Eq. (A.4), radiation becomes dominant at high temperatures, as in the case of laser cutting, and radiation is considered both on the upper and lower surfaces. Heat-transfer to the substrate is neglected. The material removal process is a rather complex interaction of the gas jet on the free surface of the melt, where shear stresses act on the cutting front and a boundary layer exists. It is assumed in the present model that any area in the molten state is expelled out of the kerf immediately by the force of the gas jet.

The CO<sub>2</sub> laser source is assumed to be of Gaussian TEM<sub>00</sub> mode. Its radial intensity distribution can then be given as  $I(r) = I(0)\exp(-4r^2/d^2)$ , where  $I(0)$  is the peak intensity,  $r$  the radial distance from the beam centre, and  $d$  equals  $2\sqrt{2}\sigma_r$ , where  $\sigma_r$  is the standard deviation of the Gaussian distribution of the laser beam intensity. Since in this work depolarised or circularly polarised laser beams are considered, as is the case coordinated motion laser cutting systems, the radial absorbed beam power is given as:

$$P_b(r) = A_b I(r) = (1 - r_f) I(r), \quad (\text{A.5})$$

where  $A_b$  is the absorptivity and  $r_f$  the reflectivity. The energy produced by the exothermic reaction is generally of the same order of magnitude as the absorbed laser beam power [14]. Assuming a pure oxygen supply for the assist gas, the following reaction occurs within the cutting kerf:  $\text{Fe} + 0.5\text{O}_2 = \text{FeO}$  and  $H = -257.58$  kJ/mol, where  $H$  is the energy released during the reaction and the ignition point is about 1470 K [15].

If the mass removal rate of the melt out of the kerf is known or can be calculated, then the following relationship can be used to determine the energy obtained by reaction:

$$P_{\text{exo}} = \text{ratio} \left( \frac{\dot{m} \Delta H}{\text{amu}} \right), \quad (\text{A.6})$$

where  $\dot{m}$  is the melt removal rate,  $\text{amu} = 1$  mole  $\text{FeO} = 71.847$  g/mol and  $\text{ratio}$  is the percentage of  $\text{FeO} : \text{Fe}$  ejected from the kerf. Because the material within the kerf is melted and then expelled it is necessary to consider latent heat effects:

$$P_{\text{melt}} = m L_f, \quad (\text{A.7})$$

where the latent heat of fusion  $L_f = 275$  kJ/kg. It has been assumed previously that the material removal rate can be given approximately by the following equation [16]

$$\dot{m} = \rho b D V_b, \quad (\text{A.8})$$

where  $b$  is the kerf width,  $D$  the workpiece thickness and  $V_b$  the velocity of the laser beam. This is only true when it is assumed that the processing speed equals the front speed as in steady-state cutting. In reality though, the front speed  $V_f$  is the factor affecting the mass removal rate and not the cutting speed. The mass removal rate is therefore more appropriately given as:

$$\dot{m} = \rho b D V_f, \quad (\text{A.9})$$

where  $V_f$  is the numerical calculation of which has been presented by Di Pietro and Yao [13], physically represents the solid–liquid interface speed, as all the molten material is assumed to be ejected from bottom of the kerf immediately. If the beam speed is too high, then melting and evaporation will cease. In this case, no melt ejection is possible and Eqs. (A.8) and (A.9) are inappropriate. This condition is continually checked throughout execution of the program and simulation ceases if it is violated. Because kerf width fluctuations are generally small for high quality cutting, it is assumed

that they are negligible and that the width is approximately of the same extent as that of the laser spot diameter. Such fluctuations have been considered elsewhere [9].

**Appendix B.**

In the case where an appropriate initial temperature distribution is required prior to cutting. Eq. (B.1) calculates the new nodal temperature at time  $j + 1$  under the implicit formulation:

Condition:  $\{X = 0 \text{ and } 0 < (Y = Y_d) < L\}$  and assist gas = oxygen

$$T_{m,n}^{j+1} = \frac{T_{m,n}^j + \sigma \left[ \frac{H}{KD} + T_{m-1,n}^{j+1} + T_{m+1,n}^{j+1} + 2T_{m,n+1}^{j+1} + Bi_f \frac{T_{\infty,y}}{D} + Bi_n \frac{T_{\infty,y}}{D} + 2Bi_r \frac{T_{\infty,y}}{D} \right]}{\left( 1 + 4\sigma + \sigma Bi_f \frac{y}{D} + \sigma Bi_n \frac{y}{D} + 2\sigma Bi_r \frac{y}{D} \right)}, \tag{B.1}$$

where

$$H = P_b(0) + P_{exo} - P_{melt}, \tag{B.2}$$

$$\sigma = \frac{\alpha t}{y^2}, \tag{B.3}$$

$$Bi_f = h_f y / K, \quad Bi_n = h_n y / K, \quad \text{and} \quad Bi_r = h_r y / K. \tag{B.4}$$

With cutting underway, the above equation is corrupted to the following form because of the existence of the kerf:

Condition:  $\{X = 0 \text{ and } 0 < (Y = Y_b) < L\}$  and assist gas = oxygen

$$T_{m,n}^{j+1} = \frac{T_{m,n}^j + \sigma \left[ \frac{H}{KD} + T_{m+1,n}^{j+1} + 2T_{m,n+1}^{j+1} + Bi_f T_{\infty} + Bi_f \frac{T_{\infty,y}}{D} + Bi_n \frac{T_{\infty,y}}{D} + 2Bi_r \frac{T_{\infty,y}}{D} \right]}{\left( 1 + 3\sigma + \sigma Bi_f + \sigma Bi_f \frac{y}{D} + 2\sigma Bi_r \frac{y}{D} + \sigma Bi_n \frac{y}{D} \right)}. \tag{B.5}$$

**References**

- [1] P. Di Pietro, Y.L. Yao, An investigation into characterizing and optimizing laser cutting quality-a review, *Int. J. Mach. Tools Manufact.* 34(2) (1994) 225–243.
- [2] J.N. Gonsalves, W.W. Duley, Cutting thin metal sheets with the CW CO<sub>2</sub> laser, *J. Appl. Phys.* 43(11) (1972) 4684–4687.
- [3] J. Powell, A. Ivarson, C. Magnusson, Laser cutting of steels: A physical and chemical analysis of the particles ejected during cutting, *J. Laser Appl.* 5(1) (1993) 25–31.
- [4] I. Miyamoto, H. Maruo, Y. Arata, Intensity profile measurements of focussed CO<sub>2</sub> laser beam using PMMA, *ICALEO, LIA 44* (1984) 313–320.
- [5] I. Miyamoto, H. Maruo, Y. Arata, Beam absorption mechanism in laser welding, laser processing: fundamentals, applications, and systems engineering, *SPIE 668* (1986) 11–18.
- [6] U. Schreiner-Mohr, F. Dausinger, H. Hugel, New aspects of cutting with CO<sub>2</sub> lasers, *ICALEO, SPIE 1722* (1991) 263–272.
- [7] S.F. Yuan, M. Querry, C. Bedrin, Thermal modelisation of laser cutting process, *Laser Technologies in Industry, SPIE 952* (1988) 583–591.
- [8] Y. Arata, H. Maruo, I. Miyamoto, S. Takeuchi, Dynamic behaviour in laser gas cutting of mild steel, *Trans. JWRI 8*(2) (1979) 15–26.
- [9] P. Di Pietro, Y.L. Yao, A new technique to characterize and predict laser cut striations, *Int. J. Mach. Tools Manufact.* 35(7) (1995) 903–1002.
- [10] M. Moriyasu, S. Hiramoro, S. Hoshinouchi, M. Ohmine, Adaptive control for high-speed and high-quality laser cutting, *Proc. ICALEO'85, 1996*, pp. 129–136.
- [11] S. Biermann, M. Geiger, Integration of diagnostics in high power laser systems for optimisation of laser material processing, *Modeling and Simulation of Laser Systems II, SPIE 1415* (1991) 330–341.
- [12] B.S. Yilbas, R. Davies, Z. Yilbas, Study into penetration speed during CO<sub>2</sub> laser cutting of stainless steel, *Optics and Lasers in Engineering, J. Eng. Manufact.* 17 (1992) 69–82.
- [13] P. Di Pietro, Y.L. Yao, A numerical investigation into cutting front mobility in CO<sub>2</sub> laser cutting, *Int. J. Mach. Tools Manufact.* 35(5) (1995) 673–688.
- [14] J. Powell, A. Ivarson, J. Kamalu, G. Borden, C. Magnusson, The role of oxygen purity in laser cutting of mild steel, *ICALEO, SPIE 1990* (1992) 433–442.
- [15] M. Geiger, H.W. Bergmann, R. Nuss, Laser cutting of steel sheets, *Laser Assisted Processing, SPIE 1022* (1988) 20–33.
- [16] D. Schuocker, Heat conduction and mass transfer in laser cutting, *Laser Technologies in Industry, SPIE 952* (1988) 592–599.
- [17] F.M. White, *Heat and Mass Transfer*, Addison-Wesley, Reading, MA, 1988, pp. 332–336.